J Solid State Electrochem (2011) 15:1919–1926
DOI 10.1007/s10008-010-1211-9

ORIGINAL PAPER

Preparation and characterization of $Bi_{0.75}Er_{0.25}O_{1.5}$ and $Bi_{0.75}Er_{0.125}Y_{0.125}O_{1.5}$ nanocrystalline ceramics by SPS

Rong Li · Qiang Zhen · Xionggang Lu · Michel Drache · Rose-Noëlle Vannier

Received: 30 June 2010 / Revised: 25 September 2010 / Accepted: 28 September 2010 / Published online: 16 October 2010

Abstract Nanopowders of $Bi_{0.75}Er_{0.25}O_{1.5}$ and $Bi_{0.75}Er_{0.125}Y_{0.125}O_{1.5}$ were prepared by a reverse titration chemical coprecipitation method under controlled pH conditions. After calcination at 500 °C for 3 h, powders with grain size in the order of 10 nm were obtained. In order to keep the nanosize of grains, these powders were densified by spark plasma sintering. Samples with relative density higher than 96% were prepared in only 10 min up to 500 °C with an average grain size of 15 and 11 nm for $Bi_{0.75}Er_{0.25}O_{1.5}$ and $Bi_{0.75}Er_{0.125}Y_{0.125}O_{1.5}$, respectively. Impedance spectroscopy revealed slightly higher conductivity for the $Bi_{0.75}Er_{0.125}Y_{0.125}O_{1.5}$ composition compared to $Bi_{0.75}Er_{0.25}O_{1.5}$ nanoceramic, but performances remained lower than the corresponding $Bi_{0.75}Er_{0.25}O_{1.5}$ microcrystalline sample. However, mechanical properties of both nanocrystalline ceramics are improved when compared to microcrystalline samples.

Keywords Bi_2O_3–Er_2O_3 · Bi_2O_3–Er_2O_3–Y_2O_3 · Nanocrystalline ceramic · SPS · Ion conductivity · Mechanical properties

R. Li · Q. Zhen (✉)
Nano-science and Nano-technology Research Center,
Shanghai University,
Shanghai 200444, People's Republic of China
e-mail: zhenqiang@263.net

R. Li · Q. Zhen · X. Lu
School of Materials Science and Engineering,
Shanghai University,
Shanghai 200444, People's Republic of China

R. Li · M. Drache · R.-N. Vannier
Unité de Catalyse et de Chimie du solide, CNRS UMR 8181,
Ecole Nationale Supérieure de Chimie de Lille,
Univ. Lille Nord de France,
59652 Villeneuve d'Ascq Cedex, France

Introduction

δ-Bi_2O_3 exhibits the highest oxide ion conductivity known up to now [1]. It is about two orders of magnitude higher than YSZ at corresponding temperature [2]. However, this δ-form is only stable from 730 °C to 825 °C [3]. It can be stabilized at room temperature by doping with other metal oxides, but this leads to a decrease of the conductivity which is due to a mismatch in ionic radii between the host and dopant cations. Among various dopants, lanthanides were extensively studied as an effective additive. In general, better performances were obtained for δ-form containing the lowest amount of dopant. With conductivities of 0.023 S cm^{-1} at 500 °C and 0.37 S cm^{-1} at 700 °C, $Bi_{0.8}Er_{0.2}O_{1.5}$ was among the best [4]. In addition, it was also found that conductivity could be improved by co-doping [5, 6], which allowed stabilization of δ-phase with a lower total dopant concentration compared to single-dopant system. For instance, higher conductivities than $Bi_{0.8}Er_{0.2}O_{1.5}$ were obtained for Dy_2O_3- and WO_3-doped Bi_2O_3 [7].

Because of their lack of stability, these materials cannot be used as electrolyte for solid oxide fuel cells, but they could find application in oxygen pump to separate oxygen from air. In this context, BIMEVOX materials which derive from the parent compound $Bi_4V_2O_{11}$ were extensively studied [8, 9].

For the applications, dense ceramics are usually needed, which can be achieved with very thin powder, especially with nanopowder with grain size at the nanoscale [10]. Moreover, when using rapid sintering technique such as spark plasma sintering (SPS), one can expect to maintain the nanosize of grains in the dense ceramic. An advantage of ceramics with grain size at the nanoscale is that mechanical properties are usually improved which is

benefit to the application [11], but electrical properties may also be influenced.

In this work, with the aim to compare the electrical and mechanical properties of bismuth-based nanocrystalline ceramics with microcrystalline ceramics, nanopowders of $Bi_{0.75}Er_{0.25}O_{1.5}$ and $Bi_{0.75}Er_{0.125}Y_{0.125}O_{1.5}$ were prepared by a reverse titration chemical coprecipitation method [12]. Using SPS, ceramics with nanograins were obtained and their electrical and mechanical properties were compared to microcrystalline materials of same composition.

Experimental

Preparation

Analytical pure Bi_2O_3, Er_2O_3, and Y_2O_3 were used as raw materials, and prior to using, Bi_2O_3 was annealed at 600 °C for one night in order to remove the carbonates and the adsorbed water. Nanopowders were prepared as described in [12]. Calcination was carried out at 500 °C for 3 h to yield nanopowders of $Bi_{0.75}Er_{0.25}O_{1.5}$ and $Bi_{0.75}Er_{0.125}Y_{0.125}O_{1.5}$.

Powders were sintered by SPS (Dr. Sinter 2080 instrument, Syntex Inc., Japan) at the French National platform in Toulouse. About 0.8 g of nanopowder was poured into a graphite die with an inner diameter of 8 mm. To avoid any contamination, the die walls were protected with graphite foils. The SPS apparatus was run under temperature control. The heating process was controlled by a K-type thermocouple put in a hole on the side of the graphite die. Experiments were carried out under pulsed DC current with a 12–2 sequence, 12 pulses of 3.3 ms spaced with two dead pulses. The period was therefore of 14×3.3 ms. During the experiment, the intensity reached 240 A at maximum.

Microcrystalline $Bi_{0.75}Er_{0.25}O_{1.5}$ and $Bi_{0.75}Er_{0.125}Y_{0.125}O_{1.5}$ ceramics were synthesized by solid reaction: Analytical pure Bi_2O_3, Er_2O_3, and Y_2O_3 were homogeneous mixed in desired ratio and annealed at 800 °C for 8 h, three times with intermediate grindings. To prepare dense ceramics, powders were pressed into pellets of 10 mm in diameter and 2 mm in thickness at an uniaxially pressure of 170 MPa. Green bodies were sintered at 900 °C for 2 h with a heating rate of 5 °C/min; ceramics with density of about 93% were obtained.

Materials characterization

As prepared, nanopowders and sintered samples were analyzed by a D8 Advance AXS Bruker diffractometer equipped with a Vantec-1 detector ($\lambda_{CuK\alpha}$= 1.5406 Å). Data were collected in the $20° \leq 2\theta \leq 80°$ domain, with a 0.0148° step size and a counting time of 0.5 s per step (a diagram was collected in 42′05″). A LaB_6 standard was used to derive the instrument resolution. The average grain size was calculated using the Scherrer equation $D = 0.89\lambda/(\beta\cos\theta)$, where β is the full width at half maximum of Bragg peaks.

Precise compositions of nanopowders were analyzed using a Shimadzu XRF-1800 apparatus. For measurement, nanopowders were pressed into disk-shape pellets with a diameter of 10 mm.

The morphology of nanopowders and sintered samples were observed using transmission electron microscopy (TEM; HITACHI H-800) and high-resolution scanning electron microscopy (SEM; JSM-6700F), respectively.

Alternating current impedance spectroscopy measurements were carried out using a computer-controlled Solartron 1255 frequency response analyzer. A gold paste was used for electrodes. It was painted on both faces of the disk-shape samples and annealed at 400 °C for 30 min (prior to the annealing, a thermogravimetric analysis was carried out

Table 1 Solubility product constant (*K*sp) [14] of possible precipitates and pH value of precipitation at 25 °C

	Solubility product constant (*K*sp)	pH value for corresponding species in the aqueous solution at the initial stage of the precipitation $C_{Bi^{3+}} = 0.075$ mol/L; $C_{Er^{3+}} = 0.025$ mol/L or $C_{Bi^{3+}} = 0.075$ mol/L; $C_{Er^{3+}} = 0.0125$ mol/L $C_{Y^{3+}} = 0.0125$ mol/L	pH range for corresponding species in the aqueous solution at the end of precipitation $C_{Bi^{3+}}$, $C_{Er^{3+}}$, $C_{Y^{3+}} \leq 10^{-5}$ mol/L
$Bi(OH)_3$	4.0×10^{-31}	4.24	5.53
BiOOH	4.0×10^{-10}	5.73	9.60
$Er(OH)_3$	4.1×10^{-24}	6.73 ($C_{Er^{3+}} = 0.025$ mol/L)	7.87
		6.84 ($C_{Er^{3+}} = 0.0125$ mol/L)	
$Y(OH)_3$	3.2×10^{-25}	6.47 ($C_{Y^{3+}} = 0.0125$ mol/L)	7.50

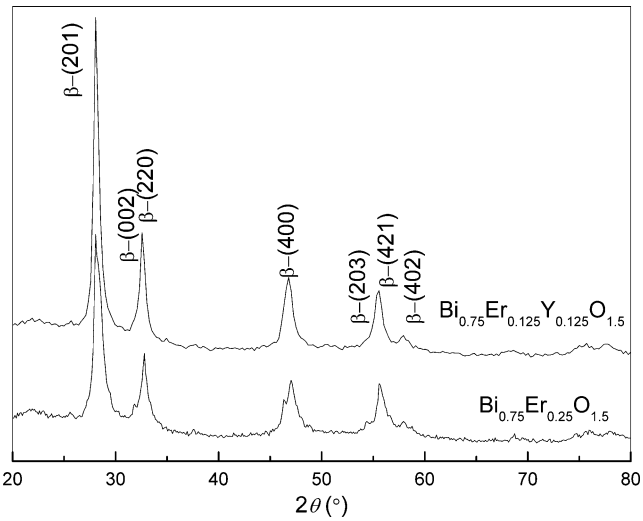

Fig. 1 XRD patterns of **a** $Bi_{0.75}Er_{0.25}O_{1.5}$ and **b** $Bi_{0.75}Er_{0.125}Y_{0.125}O_{1.5}$ after calcination at 500 °C for 3 h

on the gold paste to define the lowest temperature of annealing to be sure that all organics in the paste will be decomposed and to avoid grain growth). For impedance spectroscopy, pellets were placed between two gold electrodes using a home-made setup. A thermocouple was positioned close to the sample to monitor the temperature, increasing from 200 °C to 575 °C at 25 °C intervals. The frequency range was 1 Hz–1 MHz and the signal amplitude was 200 mV.

Vickers hardness (*H*V) of sintered samples was measured by indentions on a microhardness tester (HVS-1000) at a load of 1 kg and a dwell time of 10 s.

$$H\mathrm{V} = 1.854P/d^2 \quad (1)$$

where P is the applied load and d is the mean length of the two diagonal lines of the indentation.

Fracture toughness is given by the values of K_{IC}. The factor K_{IC} was determined using the direct crack measurement method, corresponding to Eq. 2.

$$K_{IC} = P(\pi b)^{-3/2}(\mathrm{tg}\beta)^{-1} \quad (2)$$

where b is the length of the cracks of the indentation; β equals 68°. Five indentations were made for each sample and then the average value was calculated.

Results and discussion

Preparation of $Bi_{0.75}Er_{0.25}O_{1.5}$ and $Bi_{0.75}Er_{0.125}Y_{0.125}O_{1.5}$ nanopowders

The uniformity of powders is significantly influenced by preparation conditions, notably pH conditions. In case of Bi^{3+}, $BiONO_3$ precipitates at pH lower than 6, whereas at higher pH, BiOOH is the predominant species, as confirmed by He et al. [13]. Since nitrates are difficult to

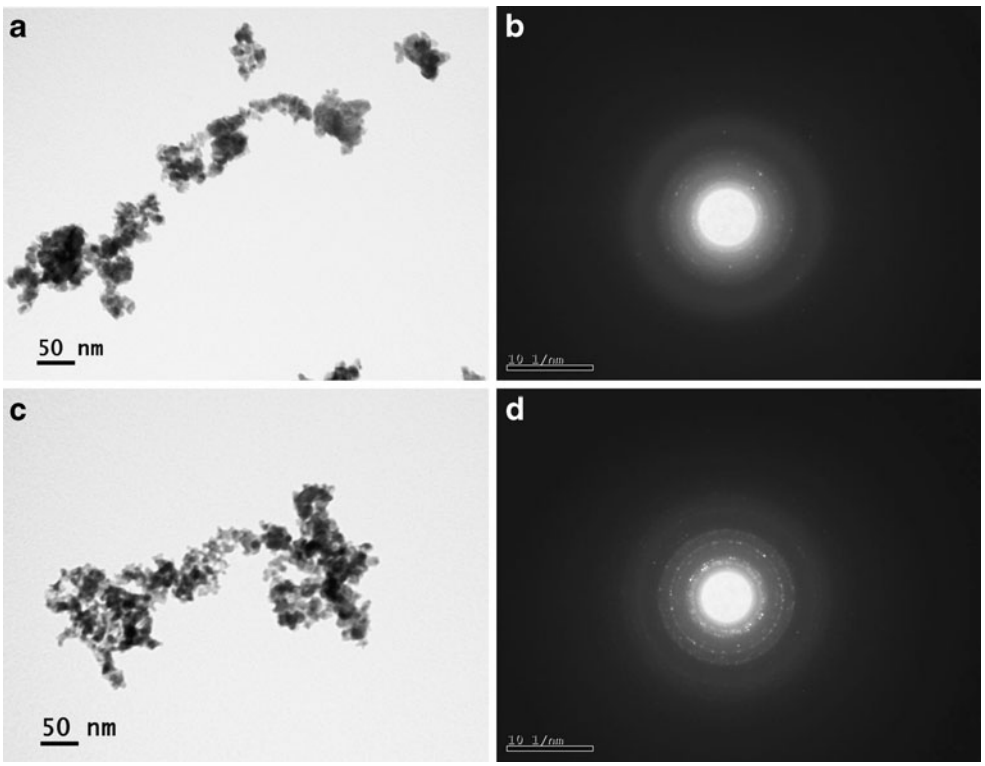

Fig. 2 TEM and electronic diffraction patterns of $Bi_{0.75}Er_{0.25}O_{1.5}$ (**a**, **b**) and $Bi_{0.75}Er_{0.125}Y_{0.125}O_{1.5}$ (**c**, **d**)

Table 2 d, I_f, and hkl of $Bi_{0.75}Er_{0.25}O_{1.5}$ and $Bi_{0.75}Er_{0.125}Y_{0.125}O_{1.5}$ powder

$Bi_{0.75}Er_{0.25}O_{1.5}$			$Bi_{0.75}Er_{0.125}Y_{0.125}O_{1.5}$		
d (Å)	I_f	hkl	d (Å)	I_f	hkl
3.19	100	201	3.15	100	201
1.92	10.8	400	2.82	25.2	220
1.72	12.2	203	1.71	12.2	203
1.59	9.0	402	1.59	9.0	402

decomposed, precipitation must be carried out at high pH. Compared to Bi^{3+}, the precipitation process of Er^{3+} and Y^{3+} is less complex; $Er(OH)_3$ and $Y(OH)_3$ are obtained at adequate pH value. As shown in Table 1, in order to precipitate Bi^{3+}, Er^{3+}, and Y^{3+} simultaneously, the pH value should be higher than 7.87 for $Bi_{0.75}Er_{0.25}O_{1.5}$ and 7.50 for $Bi_{0.75}Er_{0.125}Y_{0.125}O_{1.5}$. Therefore, in this experiment, the pH value was maintained at 11.5 during the precipitation process to obtain a mixture of BiOOH and $Er(OH)_3$, or BiOOH, $Er(OH)_3$, and $Y(OH)_3$, respectively. After filtration, these precipitates were annealed at 500 °C for 3 h to yield $Bi_{0.75}Er_{0.25}O_{1.5}$ and $Bi_{0.75}Er_{0.125}Y_{0.125}O_{1.5}$ nanopowders. Their corresponding X-ray patterns are given in Fig. 1. Each powder exhibits a β-phase, and the average grain size calculated by Scherrer equation was 11 and 10 nm for $Bi_{0.75}Er_{0.25}O_{1.5}$ and $Bi_{0.75}Er_{0.125}Y_{0.125}O_{1.5}$, respectively. These particle sizes were confirmed by TEM, as shown in Fig. 2, on which electron diffraction patterns are also reported. Indexation of the diffraction pattern is given in Table 2. It confirms the sample homogeneity.

Results of XRF analysis are given in Table 3. Within the experimental error, the compositions were in very good agreement with the expected values.

Sintering of $Bi_{0.75}Er_{0.25}O_{1.5}$ and $Bi_{0.75}Er_{0.125}Y_{0.125}O_{1.5}$ nanocrystalline ceramics

One of the main difficulties with bismuth-based materials is their sensitivity toward reduction. For rapid sintering conditions, to avoid grain growth, SPS was chosen as sintering technique. However, it is usually performed under vacuum. In our case, the lowest oxygen partial pressure was about 10^{-11} bar. Under this condition, at high temperature, Bi_2O_3 may easily reduce to Bi metal, which is liquid at 271 °C, according to the reaction equation which is given below:

$$2Bi_2O_3 = 4Bi + 3O_2(g) \quad (3)$$

The Gibbs energy of this reaction under standard state (ΔG_r^0) is calculated using the following equation:

$$\Delta G_r^0 = 4\Delta G_f^0(Bi) + 3\Delta G_f^0(O_2) - 2\Delta G_f^0(Bi_2O_3) \quad (4)$$

where ΔG_f^0 is the standard Gibbs free energy of each material; they are given in [15].

Under experimental condition, the Gibbs energy of this reaction (ΔG_r) is calculated as follows:

$$\Delta G_r = \Delta G_r^0 + RT\ln\left(\frac{P_{O_2}}{P^0}\right)^3 \quad (5)$$

where R is the molar gas constant, T is the absolute temperature, $P_{O_2}=10^{-11}$ bar, and P^0 is the atmospheric pressure.

The Gibbs energy of this reduction reaction is given in Fig. 3 as a function of temperature under standard state (ΔG_r^0) and under experimental condition (ΔG_r; $P_{O_2}=10^{-11}$ bar). ΔG_r^0 remains positive from room temperature to 1,000 °C, but under experimental condition, $P_{O_2}=10^{-11}$ bar, ΔG_r becomes negative for temperatures higher than 650 °C, which means that reduction of Bi_2O_3 is possible above 650 °C. According to this, the actual sintering temperature should be controlled to be lower than 650 °C. The heating process was controlled by a K-type thermocouple put in a hole on the side of the graphite die. However, according to some authors, a difference between the graphite die temperature and the sample may exist and reach about 150 °C [16]. Taking into account this parameter, the sintering temperature was limited to 500 °C.

In addition, because of high activity, nanopowder adsorbs CO_2 and H_2O in air easily, which has adverse effect on the densification. This is particularly true for bismuth-based powders. Therefore, with the aim to release adsorbed CO_2 and H_2O species, powders were treated at 300 °C (measured temperature) for 5 min prior to densification up to 500 °C. The sintering conditions are

Table 3 Weight percentage of metal oxide in $Bi_{0.75}Er_{0.25}O_{1.5}$ and $Bi_{0.75}Er_{0.125}Y_{0.125}O_{1.5}$ nanopowders annealed at 500 °C for 3 h deduced by X-ray fluorescence, compared to theoretical values

	$Bi_{0.75}Er_{0.25}O_{1.5}$		$Bi_{0.75}Er_{0.125}Y_{0.125}O_{1.5}$		
	Bi_2O_3	Er_2O_3	Bi_2O_3	Er_2O_3	Y_2O_3
Theoretical value (%)	78.50	21.50	82.14	11.22	6.64
Experiment value (%)	78.75±0.12	21.25±0.02	82.31±0.09	11.13±0.02	6.56±0.03
Ratio of cations	Bi/Er=3.01:0.99		Bi/Er/Y=3.01:0.50:0.49		

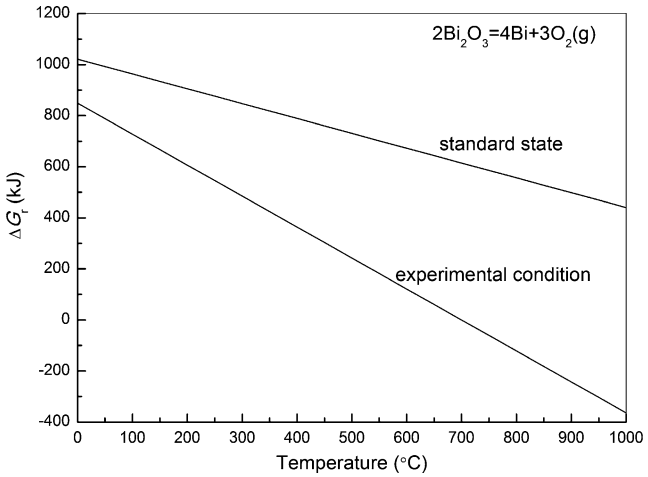

Fig. 3 ΔG_r as a function of temperature under standard state and experimental condition

given in Fig. 4. On this figure, the relative densities of both compounds as a function of time are also reported. The shrinkage behaviors of the two samples are slightly different: The maximum shrinkage rate occurred at about 400 °C (measured temperature) for $Bi_{0.75}Er_{0.25}O_{1.5}$, against 500 °C (measured temperature) for $Bi_{0.75}Er_{0.125}Y_{0.125}O_{1.5}$. However, at the end, very close relative densities of 96% were obtained for both samples.

The X-ray patterns of the dense pellets are given in Fig. 5, whereas δ-form was observed for powders, the δ-form was evidenced after densification, indicating an effect of grain size on the kinetics of transformation. Average sizes of crystallite of 15 and 11 nm were deduced for $Bi_{0.75}Er_{0.25}O_{1.5}$ and $Bi_{0.75}Er_{0.125}Y_{0.125}O_{1.5}$, respectively. Pellets were also characterized by SEM (Fig. 6). It revealed dense nanostructures with small residual porosity, with size of grains in the same order as crystallites, indicating single crystal grains.

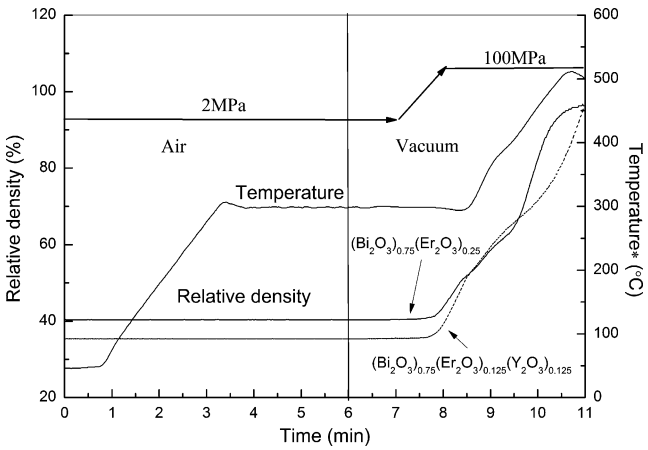

Fig. 4 Relative density and temperature* as a function of sintering time (*asterisk* temperature here is the temperature measured by the thermocouple)

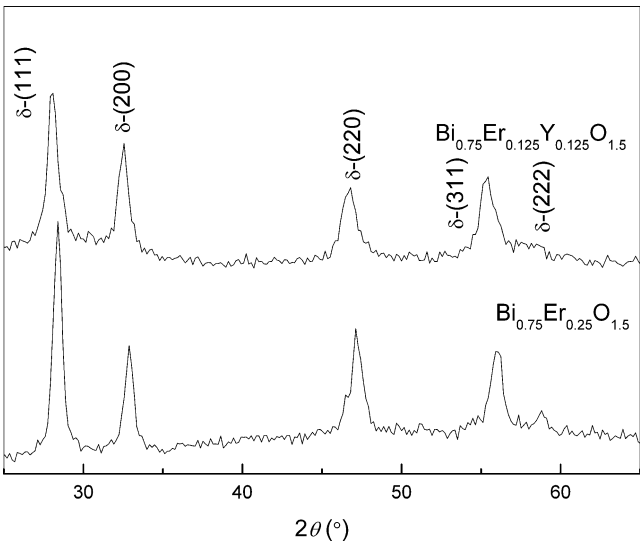

Fig. 5 XRD patterns of **a** $Bi_{0.75}Er_{0.25}O_{1.5}$ and **b** $Bi_{0.75}Er_{0.125}Y_{0.125}O_{1.5}$ nanocrystalline ceramics

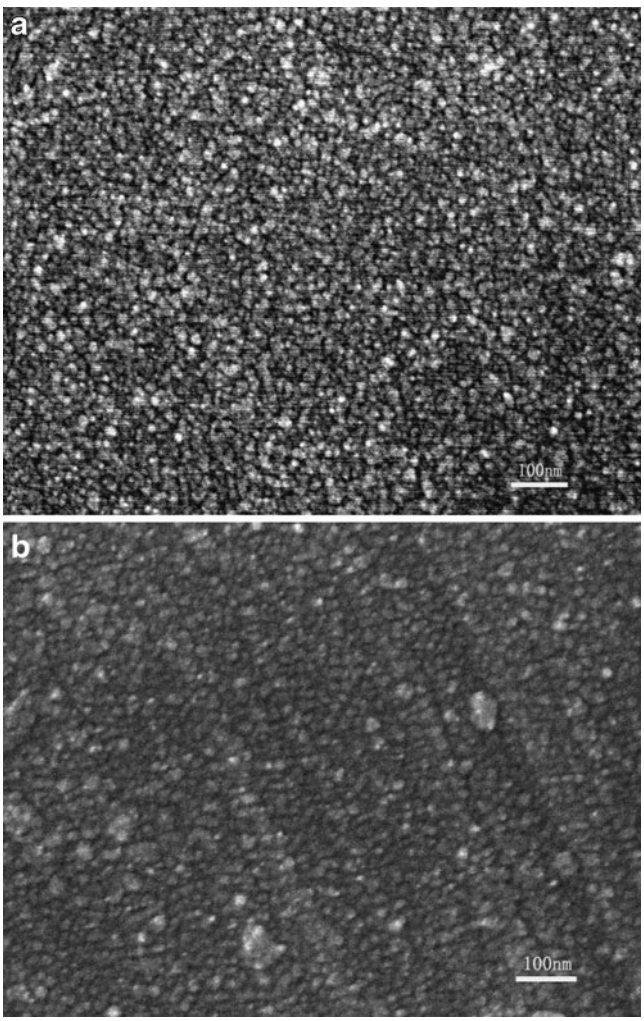

Fig. 6 Microstructure of **a** $Bi_{0.75}Er_{0.25}O_{1.5}$ and **b** $Bi_{0.75}Er_{0.125}Y_{0.125}O_{1.5}$ ceramics obtained by SPS

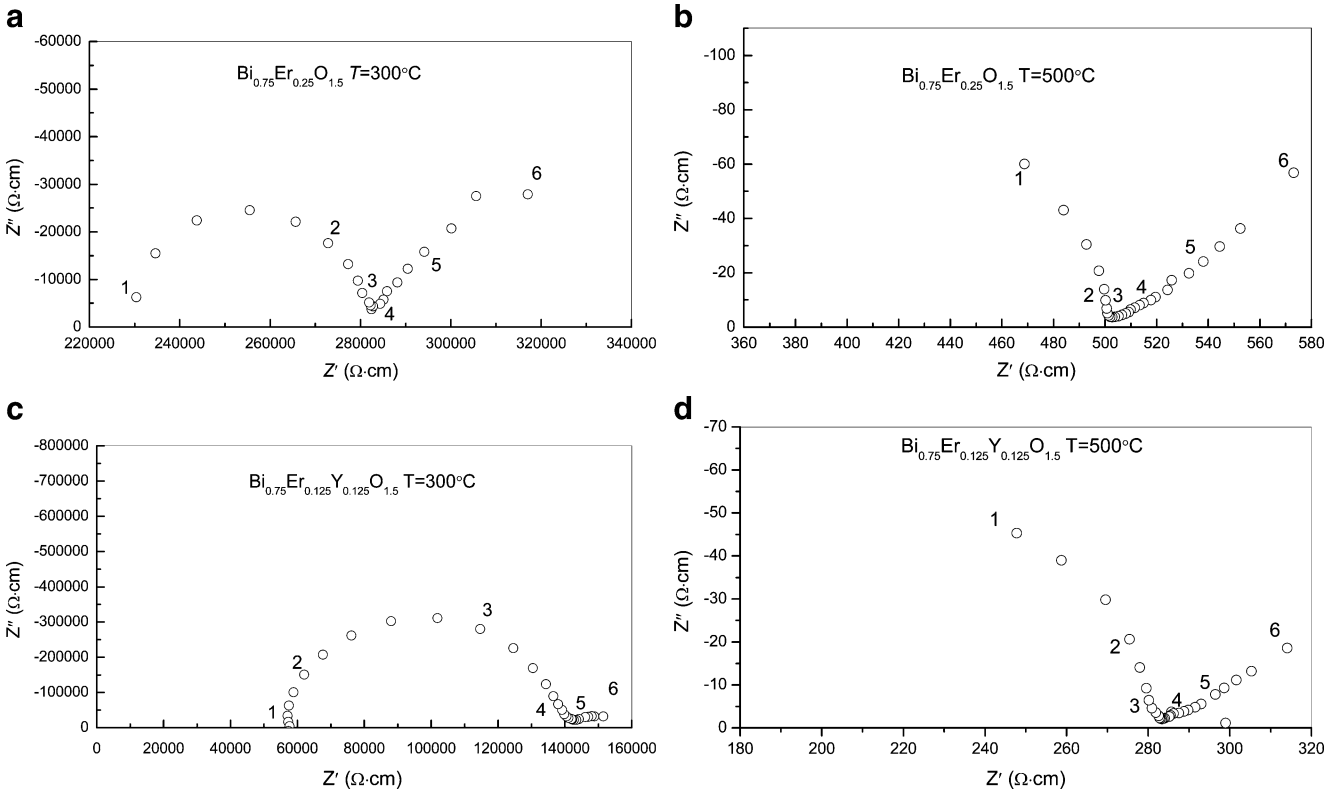

Fig. 7 Typical impedance spectrums of $Bi_{0.75}Er_{0.25}O_{1.5}$ and $Bi_{0.75}Er_{0.125}Y_{0.125}O_{1.5}$ ceramics at 300 °C and 500 °C. Digits on spectra indicated decades in frequency (it is worth noting than in the experimental setup; a reference electrode was used to measure the current which explains the shift of impedance spectra along the real axis)

Ion conductivity

Typical impedance spectra of $Bi_{0.75}Er_{0.25}O_{1.5}$ and $Bi_{0.75}Er_{0.125}Y_{0.125}O_{1.5}$ nanocrystalline ceramics collected at 300 °C and 500 °C are given in Fig. 7. It is worth noting than in the experimental setup; a reference electrode was used to measure the current which explains the shift of impedance spectra along the real axis. Two circles are observed, the first corresponds to the bulk and grain boundary responses, which are difficult to separate in this case. This is due to the very close values of relaxation frequency [17]. The associated capacitance of this first circle was in the range of 10^{-10}–10^{-9} F instead of 10^{-11} F generally observed for bulk response and 10^{-9} F for grain boundaries. The similar phenomenon was also observed in Er_2O_3-, MoO_3-, and Y_2O_3-doped Bi_2O_3 [18–20]. The second circle unambiguously corresponds to the electrode response.

From the first circle, the total ion conductivity was deduced. The corresponding Arrhenius plots are shown in Fig. 8. As expected with double substitutions, slightly higher conductivities were observed for the $Bi_{0.75}Er_{0.125}Y_{0.125}O_{1.5}$ nanoceramics. This can also be explained by the effect of dopant radius on the electrical performances. Indeed, in

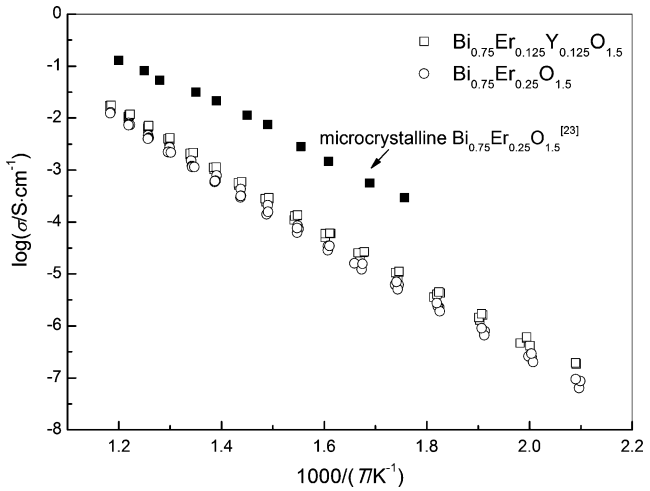

Fig. 8 Arrhenius of the conductivity for **a** $Bi_{0.75}Er_{0.25}O_{1.5}$ and **b** $Bi_{0.75}Er_{0.125}Y_{0.125}O_{1.5}$ ceramics obtained by SPS

Table 4 Effective index of sample

Molecular formula of sample	Effective index
$Bi_{0.25}Er_{0.125}Y_{0.125}O_{1.5}$	0.8368
$Bi_{0.25}Er_{0.25}O_{1.5}$	0.8290

Table 5 *Hv* and K_{IC} of nanocrystalline $Bi_{0.75}Er_{0.25}O_{1.5}$ and $Bi_{0.75}Er_{0.125}Y_{0.125}O_{1.5}$ ceramics, compared to microcrystalline samples

	$Bi_{0.75}Er_{0.25}O_{1.5}$		$Bi_{0.75}Er_{0.125}Y_{0.125}O_{1.5}$	
	Nanocrystalline %	Microcrystalline %	Nanocrystalline %	Microcrystalline %
Hv (MPa)	277±2.5	197±1.8	284±2.1	178±2.2
K_{IC} (MPa.mm$^{1/2}$)	0.57±2.2	0.52±1.9	0.52±1.7	0.48±2.0

CeO_2-based material, an effective index was defined to study the influence of crystal structure on ion conductivity [21]:

$$\text{Effective index} = (r_{ac}/r_{eo})(r_d/r_h) \quad (6)$$

where r_d is the average ionic radius of dopant, r_h is the ionic radius of host element, r_{ac} is the average ionic radius of cation, and r_{eo} is the effective oxygen ionic radius, which is given by:

$$r_{eo} = 1.4[2 - \delta/2] \quad (7)$$

where δ is the level of oxygen vacancies in the material. It was found that in CeO_2-based system, when the effective index tends to 1, the system exhibits higher ion conductivity than others. Since doped Bi_2O_3 has the same fluorite structure as CeO_2-based materials, the similar estimation can be made. Corresponding effective index is given in Table 4. A slightly higher value was effectively obtained for $Bi_{0.25}Er_{0.125}Y_{0.125}O_{1.5}$.

However, when compared with conductivity reported for microcrystalline ceramic [22], the conductivity of nanocrystalline samples is about one order of magnitude lower (see in Fig. 8). This is likely due to the great increase in volume of grain boundary with the reduction of grain size which leads to an increase of the grain boundary resistance. The same effect was also observed in yttria-doped zirconia ceramics, which exhibits the same fluorite structure as δ-Bi_2O_3 [23].

Mechanical properties

Fracture toughness property and Vickers hardness of nanocrystalline $Bi_{0.75}Er_{0.25}O_{1.5}$ and $Bi_{0.75}Er_{0.125}Y_{0.125}O_{1.5}$ ceramics were investigated and compared to those of corresponding microcrystalline with the same compositions. From Table 5, H_v of nanocrystalline samples are much higher than microcrystalline samples; an increase of about 41% for $Bi_{0.75}Er_{0.25}O_{1.5}$ and 60% for $Bi_{0.75}Er_{0.125}Y_{0.125}O_{1.5}$ is observed. A slight increase of K_{IC} is also to be noticed. This confirms an improvement of mechanical properties when the grain size is reduced. In polycrystalline material, smaller grain size means larger volume of grain boundary, which needs more energy for plastic deformation and leads to higher fracture toughness property.

Conclusion

$Bi_{0.75}Er_{0.25}O_{1.5}$ and $Bi_{0.75}Er_{0.125}Y_{0.125}O_{1.5}$ nanopowders were successfully prepared by a reverse titration chemical coprecipitation method. BiOOH, $Er(OH)_3$, and $Y(OH)_3$ were predicted as main precipitates when pH was controlled at 11.5. After calcination at 500 °C for 3 h, $Bi_{0.75}Er_{0.25}O_{1.5}$ and $Bi_{0.75}Er_{0.125}Y_{0.125}O_{1.5}$ nanopowders of β-form were obtained with average grain size of 11 and 10 nm, respectively. After sintering by SPS, δ-forms were stabilized at room temperature. Nanoceramics were obtained with average grain sizes of 15 and 11 nm, respectively, and relative densities of about 96%. Although $Bi_{0.75}Er_{0.125}Y_{0.125}O_{1.5}$ conductivity is slightly higher than $Bi_{0.75}Er_{0.25}O_{1.5}$ one, it is one order of magnitude lower than conductivity reported on microcrystalline samples of same compositions, likely because of blocking effect due to grain boundary. However, nanocrystalline samples exhibit higher Vickers hardness and fracture toughness, due to the reduction of grain size, which could be beneficial to the application.

Acknowledgment Authors are grateful to the French Embassy in China for funding R. Li grant as a co-tutorial Ph.D. between Shanghai University and the University of Lille. The authors also thank the Instrument Analysis Research Center of Shanghai University for their help in the characterization of materials (SEM, TEM, XRF) and Claude Estournes and his collaborators at the Plate-forme Nationale de Frittage Flash (PNF2) in Toulouse for their help during the sample sintering. The Leading Academic Discipline Project of Shanghai Municipal Education Commission (No. J50102), Key Project of Ministry of Education, China (No. 208043), Key Project of Shanghai Education Committee (No. 07zz10), and Magnolia Science and Technology Talent Fund (No. 2008B049) are also gratefully acknowledged for their funding.

References

1. Wachsman ED (2004) J Eur Ceram Soc 24:1281–1285
2. Huang SG, Zhou GM, Xie Y (2008) J Alloys Compd 464:322–326
3. Drache M, Roussel P, Wignacourt JP (2007) Chem Rev 107:80–96
4. Verkerk MJ, Burggraaf AJ (1981) J Electrochem Soc 128:75–82
5. Fung KZ, Virkar AV (1991) J Am Ceram Soc 74:1970–1980
6. Jiang N, Wachsman ED, Jung S (2002) Solid State Ionics 150:347–353
7. Jung DW, Duncan KL, Wachsman ED (2010) Acta Mater 58:355–363

8. Boivin JC, Pirovano C, Nowogrocki G, Mairesse G, Labrune P, Lagrange G (1998) Solid State Ionics 113:639–651
9. Pirovano C, Vannier RN, Capoen E, Nowogrocki G, Boivin JC, Mairesse G, Anne M, Doryhee E, Strobel P (2003) Solid State Ionics 159:167–179
10. Kim GS, Kim HG, Kim DG, Oh ST, Suk MJ, Kim YD (2009) J Alloys Compd 469:401–405
11. Wang JT, Yin DL, Liu JQ, Tao J, Su YL, Zhao X (2008) Scr Mater 59:63–66
12. Li R, Zhen Q, Drache M, Rubbens A, Vannier RN (2010) J Alloys Compd 494:446–450
13. He W, Zhen Q, Pan Q, Liu J (2003) Function material (China) 6:702–706
14. Stephen H, Stephen T (1963) Solubilities of inorganic compounds, vol. 1. Pergamon, Oxford
15. Ihsan B (2003) Thermochemical data of pure substances. Science, Beijing
16. Wada S, Suganuma M, Kitagawa Y, Murayama N (1999) J Ceram Soc Jpn 107:887–890
17. Wang CZ (2000) Solid electrolyte and chemical sensors. Metallurgical Industry, Beijing
18. Macdonald JR (1987) Impedance spectroscopy. Wiley, New York
19. Duran P, Jurado JR, Moure C, Valverde N, Steele BCH (1987) Mater Chem Phys 18:287–294
20. Wang LS, Barnett SA (1992) J Electrochem Soc 139:2567–2572
21. Mori T, Drennan J, Wang Y, Li JG, Ikegami T (2002) J Therm Anal Calorim 70:309–319
22. Nakayama S (2002) Ceram Int 28:907–910
23. Boulfrad S, Djurado E, Dessemond L (2008) Fuel Cells 5:313–321